Proceedings of OMAE 2008
27th International Conference on Offshore Mechanics and Arctic Engineering
Estoril, Portugal, June 15-20, 2008

OMAE2008-57129

ENVELOPE AND PHASE STATISTICS OF LARGE WAVES

M. Aziz Tayfun
College of Engineering & Petroleum, Kuwait University
aziztayfun@usa.net

Francesco Fedele
School of Civil & Environmental Engineering
Georgia Institute of Technology, Savannah, USA

ABSTRACT

A theoretical expression derived previously for describing the joint distribution of the envelope and phase of nonlinear waves is verified with wind-wave measurements collected in the North Sea. The same distribution is explored further to derive the marginal and conditional distributions of wave envelopes and phases. The nature and implications of these are examined with emphasis on the occurrence of large waves and associated phases. It is shown that the wave-phase distribution assumes two distinct forms depending on whether if envelope elevations exceed the significant envelope height or not. For envelope elevations sufficiently larger than this threshold, the wave-phase distribution approaches a simple limit form, indicating that large surface displacements can occur only above the mean sea level. Comparisons with the North Sea data confirm these theoretical results and also suggest that large surface displacements and thus large wave heights arise from the constructive interference of spectral components with different amplitudes and phases. Further, large waves with high and sharp crests do not display any secondary maxima and minima. They appear more regular or narrow-banded than relatively low waves, and their heights and crests do not violate the Miche-Stokes type upper limits.

INTRODUCTION

Suppose that the sea surface displacement $\eta(t)$ measured from the mean sea level at a fixed point in time t and its conjugate or Hilbert transform $\hat{\eta}(t)$ are both normalized with their root-mean-square σ. They can then be represented as the real and imaginary parts of the complex process

$$\xi \exp(i\,\phi) = \eta + i\,\hat{\eta} = \xi \cos\phi + i\xi \sin\phi\,, \tag{1}$$

where $\xi(t)$ and $\phi(t)$ define the wave envelope and phase. The explicit expressions for η and $\hat{\eta}$ characterized with second-order nonlinearities are given in Tayfun (1994). These and the theoretical statistics developed from them, including the distributions of η and $\hat{\eta}$ expanded in Gram-Charlier series, related third-order cumulants and thus the resulting probability structure of ξ and ϕ are all valid for directional wind seas at deep and transitional water depths, although Tayfun (1994) elaborates them only for deep-water waves.

To the leading order of approximation, η is linear Gaussian, and the probability density (p.d.) describing ξ and ϕ jointly assumes the form (Rice 1944, 1945)

$$p_{\phi\xi} = p_{\phi}.\,p_{\xi} = (1/2\pi)\;.\;\xi\;\exp(-\xi^{\,2}/2)\;. \tag{2}$$

Thus, ϕ and ξ are statistically independent, ϕ by itself is uniformly random, say in $(-\pi, \pi)$, and the envelope ξ Rayleigh-distributed.

In the second-order approximation, η is weakly nonlinear and non-Gaussian, and (2) is modified as (Tayfun 1994)

$$\begin{aligned} p_{\phi\xi} &= p_{\phi\,|\,\xi}\,.\,p_{\xi} \\ &= \frac{1}{2\pi}\,[1+\frac{\lambda_3}{6}\xi(\xi^2-4)\cos\phi]\;.\;\xi\,\exp(-\xi^2/2), \end{aligned} \tag{3}$$

where $\lambda_3 =< \eta^3 > \equiv$ skewness coefficient. This result is identical to earlier approximations derived in Tayfun & Lo (1989, 1990) under less general conditions. It also suggests a somewhat more complex structure where ϕ and ξ are no longer statistically independent since $p_{\phi\xi} \neq p_{\phi}\,.\,p_{\xi}$.

Some characteristics and implications of (3), such as the marginal distributions describing ϕ and ξ by themselves have previously been explored and compared in Tayfun & Lo (1989, 1990) and Tayfun (1994) with simulations and measurements gathered at a relatively poor sampling rate of 1 Hz in the Gulf of Mexico during the passage of hurricane Camille in 1969. One of the objectives here is to have a closer look at (3) itself and to compare it with more recent measurements from the North Sea. The same expression is then used to obtain various theoretical expressions describing the conditional distributions of ϕ and ξ, with emphasis on large surface displacements and the nature of associated phases. Some limited comparisons similar to those in the previous studies aforementioned are also given as a further verification of theoretical results and for completeness of presentation. The validity of Miche-Stokes type bounds that limit the occurrences of large wave heights and crests, and possible effects due to higher-order nonlinearities such as the third-order quasi-resonant interactions elaborated in Socquet-

Juglard et al. (2005), Mori & Janssen (2006) and Mori et al. (2007) are also considered briefly.

DATA

The measurements that will be used for verifying various theoretical results comprise 9-h measurements gathered at 4 Hz with a Baylor wave staff from the Meetpost Noordwijk platform in 18 m average water depth in the southern North Sea in January, 1998 as part of the Wave Crest Sensor Inter-comparison Study (Forristall et al. 2002). This data, hereafter referred to as WACSIS, represents fairly energetic waves at a transitional water depth. The frequency spectral density of surface displacements is representative of typical wind seas, tending to a ω^{-4} power law for frequencies larger than approximately 1~2 times the spectral-peak frequency.

The variations of σ and λ_3 estimated from half-hourly segments are shown in Fig. 1. WACSIS exhibits relatively strong non-stationary and nonlinear characteristics. The segmental σ estimates differ from the overall average $\sigma_{avg} = 0.981$ m by as much as $\pm 17\%$; and, $\lambda_{3avg} = 0.236$ as an overall average, but the half-hourly samples vary from 0.172 to 0.278. To compensate for non-stationarity at least partially, all analyses will be done in half-hourly segments, scaling all elevations in each segment with the corresponding σ.

JOINT DISTRIBUTION

For $\lambda_3 = 0.3$ as a hypothetical case, the joint p.d. (3) is illustrated in Fig. 2 as contours of $2\pi\, p_{\phi\xi}$. These differ noticeably from the corresponding contours of (2) for linear waves because if the latter were plotted in the same figure, they would appear as parallel lines.

It is noted that $p_{\phi\,\xi} < 0$ in $\Omega \equiv \{\phi_c < |\,\phi\,| \le \pi\,,\ \xi > \xi_m\}$, where

$$\phi_c = \cos^{-1}[-6/\lambda_3\,\xi(\xi^2-4)]\ ;\ \ \xi > \xi_m\,, \tag{4}$$

and ξ_m is such that

$$1-\frac{\lambda_3}{6}\,\xi_m\,(\xi_m^2-4) = 0\,. \tag{5}$$

In general, $\xi_m > 2$ and follows easily in a few iterations from $\xi_{m,\,j+1} = [(6/\lambda_3) + 4\,\xi_{m,\,j}\,]^{1/3}$, with j = 0, 1, 2, … and $\xi_{m,0} = 2$. Clearly, the values of ϕ and ξ in Ω lie above the curves $\pm\phi_c$. Oceanic values of λ_3 are typically less than 0.3. And, numerical computations for $0.05 < \lambda_3 \le 0.5$ indicate that the probability mass over Ω is less than 10^{-3} in absolute value. So, the non-negativity issue is not significant for (3), but it will be so later in considering the conditional p.d. of ϕ, given ξ,

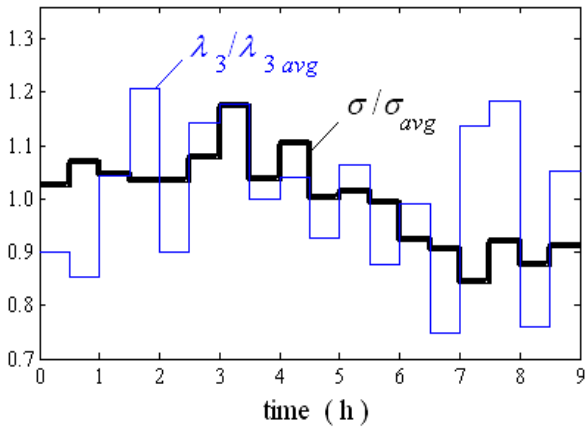

Fig. 1. Half-hourly variations of σ and λ_3 in WACSIS: $\sigma_{avg} = 0.981$ m and $\lambda_{3avg} = 0.236$.

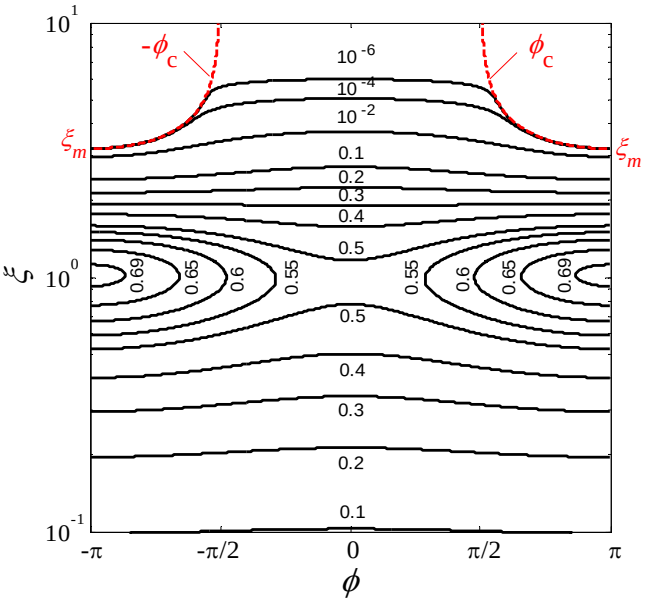

Fig. 2. Contours of $2\pi\, p_{\phi\xi}$ = constant from (3) for $\lambda_3 = 0.3$.

whenever $\xi > \xi_m$.

The contours of $2\pi\, p_{\phi\xi}$ observed in WACSIS are compared with the corresponding predictions from (3) in Fig. 3. Evidently, (3) represents the observed data reasonably well. The curves $\pm\phi_c$ based on the overall average $\lambda_{3avg} = 0.236$, and the scatter of wave phases and associated envelopes derived from half-hourly segments are also shown in Fig. 4 for $\xi > 2$. It is seen that if $\xi > \xi_m$, then the physically realizable ϕ tend to lie in $(-\phi_c, \phi_c)$. Further, $\phi_c \to \pi/2$ and $\Pr\{\eta > 0\} \to 1$ as $\xi \to \infty$. Thus, exceptionally large surface displacements can occur only above the mean sea level. In linear waves, surface

displacements, no matter how large, are equally likely both above and below the mean level.

Also shown in Fig. 4 are the envelopes and phases associated with the two largest surface displacements denoted as η_1 and η_2, respectively. The corresponding wave heights, envelopes, phases and conjugates are $h_1 = 9.270$, $\xi_1 = 6.042$, $\phi_1 = -0.028$ and $\hat{\eta}_1 = -0.171$ for $\eta_1 = 6.039$; and, $h_2 = 7.955$, $\xi_2 = 5.050$, $\phi_2 = 0.347$ and $\hat{\eta}_2 = 1.715$ for $\eta_2 = 4.749$. The largest four envelope heights in Fig. 3 congregate around the crest of the largest wave. In general, the largest surface displacement does not necessarily occur simultaneously with the largest envelope height, as seen in this figure, but it does so if $\phi \cong 0$ also. In theory, the latter condition implies wave focusing, viz. the constructive interference or superposition of a sufficiently large number of wave components when their phases approach 0 simultaneously. In wind seas, this is the most likely process that causes large surface displacements and unusually large waves with scaled features and proportions quite similar to the largest wave in WACSIS, often referred to as freak or rogue waves.

MARGINAL DISTRIBUTIONS

The marginal p.d..s describing ξ and ϕ by themselves follow by integration from (3) as

$$p_\xi = \xi \exp(-\xi^2/2), \tag{6}$$

$$p_\phi = \frac{1}{2\pi}\left\{1 - \frac{\lambda_3}{6}\sqrt{\frac{\pi}{2}}\cos\phi\right\}. \tag{7}$$

The marginal p.d. (6) is of the Rayleigh form, as in linear waves. However, the nonlinear surface is vertically skewed, with higher and sharper crests, and shallower and more rounded troughs. Accordingly, wave envelopes are expected to be higher and narrower over the crest segments where $\eta > 0$, and shallower and wider over the troughs segments where $\eta \le 0$. Overall, such opposing distortions do not affect the marginal distribution of wave envelopes, particularly in the absence of higher-order nonlinear effects such as third-order quasi-resonant interactions among free waves that amplify the wave envelopes over both crest and trough segments (Socquet-Juglard et al. 2005, Mori & Janssen 2006, Mori et al. 2007). As shown in Fig. 5, both expressions compare favorably with the WACSIS data for the most part. Discrepancies between the observed and predicted p.d.s do appear for $\xi > 4$ and $p_\xi < 10^{-4}$, as the data become rather sparse.

Note that $\eta > 0$ if $|\phi| \le \pi/2$, and $\eta \le 0$ otherwise. Thus, $P^+ \equiv \Pr\{\eta > 0\}$ and $P^- \equiv \Pr\{\eta \le 0\} = 1 - P^+$ follow

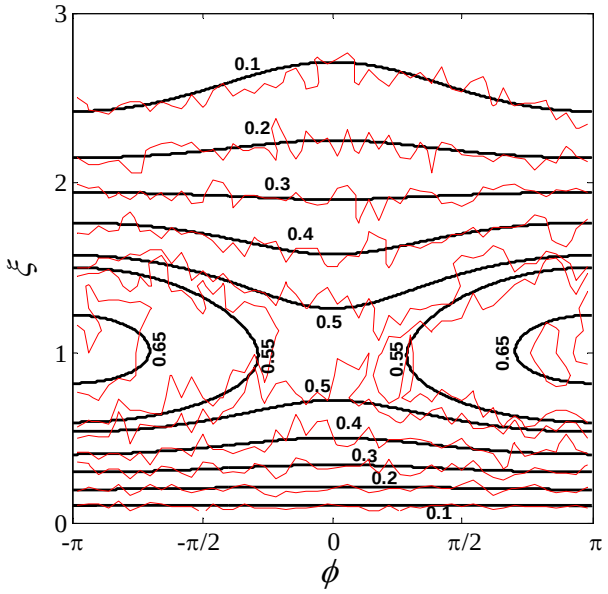

Fig. 3. Contours of $2\pi\, p_{\phi\xi}$ from WACSIS (red) and (3).

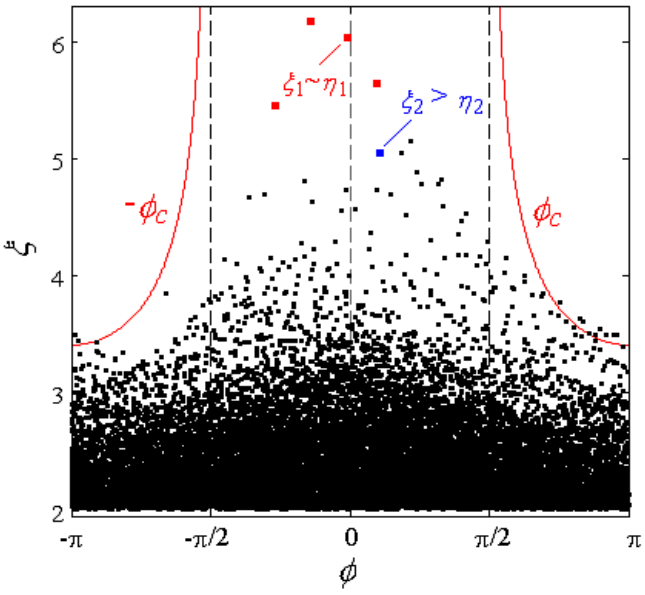

Fig. 4. The scatter diagram of ϕ and $\xi > 2$ from WACSIS: envelope(s) & phase(s) of the two largest waves and their crests

by integration from (7) as

$$P^\pm = \frac{1}{2}\left(1 \mp \frac{\lambda_3}{3\sqrt{2\pi}}\right). \tag{8}$$

By definition, $P^+ + P^- = 1$, but $P^- > 1/2$ and $P^+ < 1/2$ for

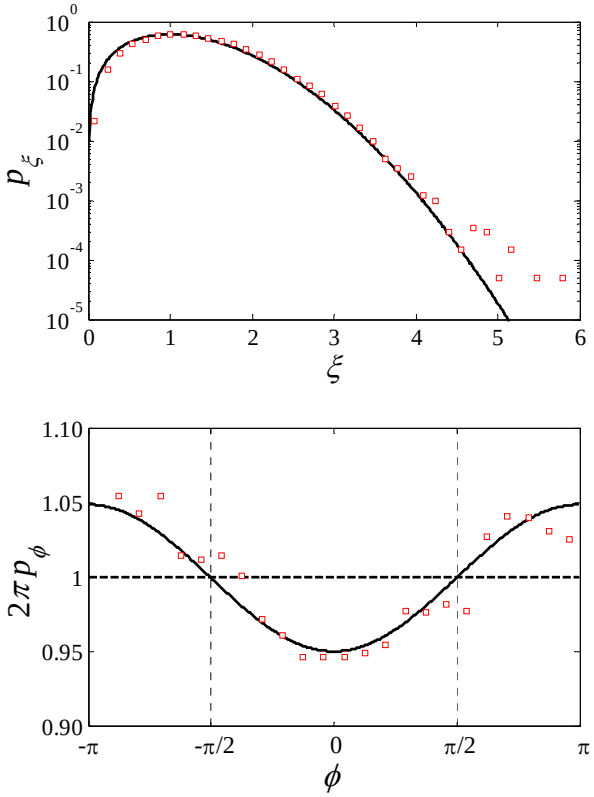

Fig. 5. Marginal p.d.s of ξ and ϕ observed in WACSIS (points) versus approximations (6) & (7) (continuous curves).

$\lambda_3 > 0$. Thus, the sea surface stays somewhat longer below the mean sea level than it does above it. Further, (8) can be used to estimate λ_3 from a zero-mean surface series directly since $\lambda_3 \cong 3\sqrt{2\pi}\,(1 \mp 2P^{\pm})$. With $P^{+} \cong 0.485$ in WACSIS, the latter expression gives $\lambda_3 \cong 0.230$, which compares in this case quite well with 0.236 computed from the cubic moment of the surface time series.

CONDITIONAL DISTRIBUTIONS OF ENVELOPES

In order to describe how the wave envelope is modified by the surface skewness, it is necessary to consider its conditional distributions, given that $\eta > 0$ and $\eta \le 0$, respectively. The conditional densities sought, say, p_{ξ^+} for $\eta > 0$ and p_{ξ^-} for $\eta \le 0$ follow from (3) as (Al-Humoud et al. 2002)

$$p_{\xi^{\pm}}(x) = \beta^{\mp}\left[1 \pm \frac{\lambda_3}{3\pi}\, x\,(x^2 - 4)\right] p_\xi(x)\ , \qquad (9)$$

where $\beta^{\mp} = \left[\,1 \mp \lambda_3 \big/ 3\sqrt{2\pi}\,\right]^{-1}$. Therefore, the respective exceedance distributions (e.d.) are of the form

$$E_{\xi^{\pm}} = \beta^{\mp}\left\{1 \pm \frac{\lambda_3}{3\pi}\left[\xi(\xi^2 - 1) - \sqrt{\frac{\pi}{2}}\, e^{\xi^2/2}\, erfc(\xi/\sqrt{2})\right]\right\} E_\xi\ , \qquad (10)$$

where $E_\xi = \exp(-\xi^2/2)$ corresponds to the Rayleigh e.d., and $erfc \equiv$ complementary error function. In theory, (10) should describe crest and trough amplitudes in narrow-band waves just as the Rayleigh distribution does for linear narrow-band waves. Al-Humoud et al. (2002) and Cherneva et al. (2005) explore this possibility, but for relatively broad-band waves in deep and shallow water. Although some comparisons of (10) with shallow-water data in Cherneva et al. (2005) appear surprisingly favorable, the quantitative accuracy of such approximations is generally somewhat poor for typical wind seas with broad-band characteristics.

CONDITIONAL DISTRIBUTIONS OF WAVE PHASE

The conditional p.d. of ϕ, given ξ, follows from (3) by way of standard probabilistic definitions as

$$p_{\phi|\xi} = \frac{C_1}{2\pi}\left[1 + \frac{\lambda_3}{6}\,\xi(\xi^2 - 4)\cos\phi\right], \quad |\phi| \le \phi_c\,, \qquad (11)$$

where

$$C_1 = \left\{\begin{array}{ll} 1\,, & \xi \le \xi_m \\ \dfrac{\pi}{\phi_c - \tan\phi_c}\,, & \xi > \xi_m \end{array}\right\}\ , \qquad (12)$$

with $\xi_m > 2$ as in (4), and

$$\phi_c = \left\{\begin{array}{ll} \pi\,, & 0 < \xi \le \xi_m \\ \cos^{-1}[-6/\lambda_3\,\xi(\xi^2 - 4)]\,, & \xi > \xi_m \end{array}\right\}. \qquad (13)$$

As $\xi \to \infty$, $\phi_c \to \pi/2$ and so (13) converges to

$$p_{\phi|\xi} = (1/2)\cos\phi, \quad |\phi| \le \pi/2\,. \qquad (14)$$

The variation of $p_{\phi|\xi}$ with ξ is shown in Fig. 6 for $\lambda_3 = 0.3$. It is recalled that $\xi_s = 2 \equiv$ mean of the 1/3-rd largest ξ's, conventionally referred to as the significant value. Clearly, $p_{\phi|\xi}$ appears strikingly different depending on whether if $\xi \le \xi_s$ or not. For $\xi = 0$ *and* ξ_s, $p_{\phi|\xi}$ is uniform as in linear waves. For $0 < \xi < 2/\sqrt{3} \cong 1.15$, $p_{\phi|\xi}$ tends to deviate from the uniform p.d. $1/2\pi$ up to 1.15. As ξ increases further from 1.15 to ξ_s, it converges back to $1/2\pi$. In general,

$p_{\phi|\xi}$ displays a slight excess of phases over wave troughs and a corresponding deficiency elsewhere. However, when $\xi > \xi_s$ and as it gets larger, $p_{\phi|\xi}$ predicts a progressively increasing excess of phases over wave crests, eventually converging to the limit form (14). All this suggests that physically, the surface stays slightly longer below the mean sea level if $\xi < \xi_s$, whereas if $\xi > \xi_s$, the opposite occurs in a more pronounced manner as ξ becomes larger. In particular, the limit form (14) suggests that exceptionally large surface displacements can occur only above the mean sea level. This result is entirely consistent with the WACSIS data of Fig. 4.

The conditional p.d. $p_{\phi|\xi}$ can not be estimated from a surface time series unless the condition "given ξ" is approximated as "given $\xi - \Delta\xi < \xi \le \xi + \Delta\xi$" such that $\Delta\xi << \xi$. WACSIS comparisons shown in Fig. 7 use this approach for $\xi = 2, 3$ and 3.5 with $\Delta\xi = 0.2$. It is seen that (11) describes the wave-phase densities observed reasonably well.

The p.d. of ϕ, conditional on $A \equiv \{\xi > \xi_0\}$, is given by

$$p_{\phi|A} = \frac{C_2}{2\pi}\left\{1 + \frac{\lambda_3}{6}\, f(\xi_0)\cos\phi\right\}, \quad |\phi| \le \phi^*, \qquad (15)$$

where

$$f(\xi_0) \equiv \xi_0^3 - \xi_0 - \sqrt{\pi/2}\,\exp(\xi_0^2/2)\, erfc(\xi_0/\sqrt{2}), \qquad (16)$$

$$C_2 = \left\{\begin{array}{ll} 1, & \xi_0 \le \xi_0^* \\ \dfrac{\pi}{\phi^* - \tan\phi^*}, & \xi_0 > \xi_0^* \end{array}\right\}, \qquad (17)$$

with $\xi_0^* > 1.2176$ in general such that $f(\xi_0^*) = 6/\lambda_3$, and

$$\phi^* = \left\{\begin{array}{ll} \pi, & 0 < \xi_0 \le \xi_0^* \\ \cos^{-1}[-6/\lambda_3\, f(\xi_0)], & \xi_0 > \xi_0^* \end{array}\right\}. \qquad (18)$$

In this case, ξ_0^* follows by iteration from

$$x_{j+1} = \left[\frac{6}{\lambda_3} + x_j + \sqrt{\frac{\pi}{2}}\exp(x_j^2/2)\, erfc(x_j/\sqrt{2})\right]^{1/3} \qquad (19)$$

with j = 0, 1, 2,…, and $x_0 \ge 0$.

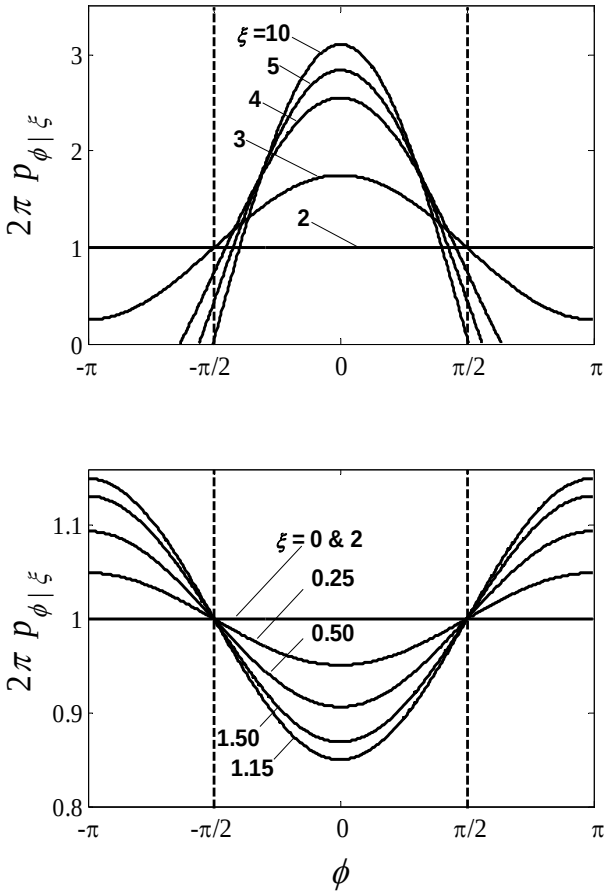

Fig. 6. The variation of the conditional p.d. $p_{\phi|\xi}$ of ϕ, given ξ, with ξ for $\lambda_3 = 0.3$.

The p.d. of ϕ, conditional on $B \equiv \{\xi \le \xi_0\}$, has the form

$$p_{\phi|B} = \frac{1}{2\pi}\left[1 - \frac{\lambda_3}{6}\, h(\xi_0)\cos\phi\right], \qquad (20)$$

where $\xi_0 > 0$, $|\phi| \le \pi$ and, with *erf* ≡ error function, and

$$h(\xi_0) = \frac{\xi_0^3 - \xi_0 + \sqrt{\pi/2}\,\exp(\xi_0^2/2)\, erf(\xi_0/\sqrt{2})}{\exp(\xi_0^2/2) - 1}. \qquad (21)$$

The functions f and h are shown in Fig. 8. In general, $h \ge 0$ with a maximum 2.5108 at $\xi_0 \cong 1.539$, whereas $f \le 0$ for $\xi_0 < 1.2176$ and $f > 0$ otherwise. As $\xi_0 \to 0$, $f \to -\sqrt{\pi/2}$

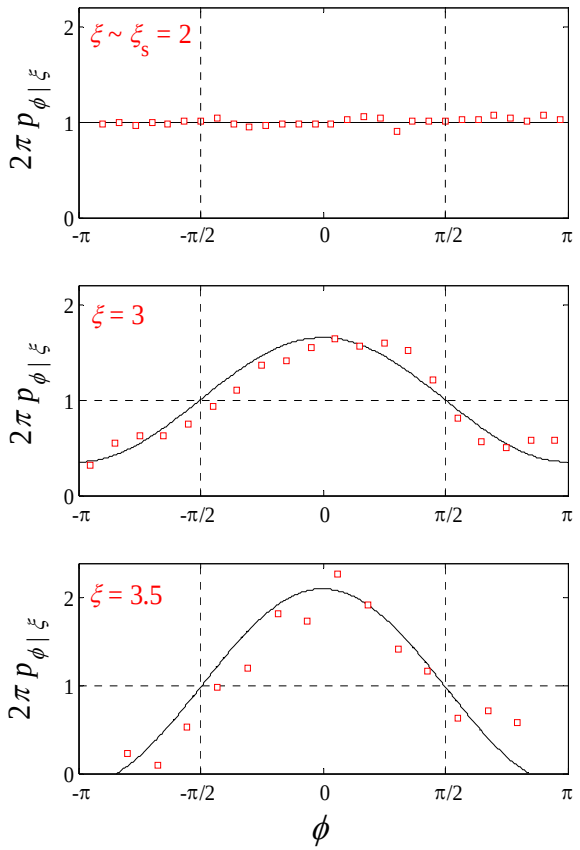

Fig. 7. Comparisons of the conditional p.d. $p_{\phi\,|\,\xi}$ of ϕ, given ξ, observed in WACSIS with (11) for $\xi = 2$, 3 and 3.5.

and $p_{\phi\,|A} \to p_{\phi}$ of (7). As $\xi_0 \to \infty$, $p_{\phi\,|A} \to (1/2)\cos\phi$; and, if $\xi_0 \cong 1.2176$, then $p_{\phi\,|A} \to 1/2\pi$ for any λ_3. In comparison, for $0 < \xi_0 << 1$, $h \approx 0$ and $p_{\phi\,|B} \approx 1/2\pi$. If, however, $\xi_0 > 4$ approximately, $h \to \sqrt{\pi/2}$ and $p_{\phi\,|B} \to p_{\phi}$ of (7) also.

The variation of the conditional p.d. $p_{\phi|A}$ in (15) with ξ_0 for $\lambda_3 = 0.3$ is shown in Fig. 9, and its comparisons with the WACSIS data in Figs. 10. Similarly, the variation of $p_{\phi|B}$ in (20), and its comparisons with WACSIS are shown in Figs. 11 and 12, respectively. Both sets of comparisons seem to validate the theoretical expressions (15) and (20) reasonably well.

To explore the nature of large surface displacements further, let $P_A^+ \equiv \Pr\{\eta > 0\,|\,A\}$ denote the conditional probability, given $A \equiv \{\xi > \xi_0\}$. By integration from (15),

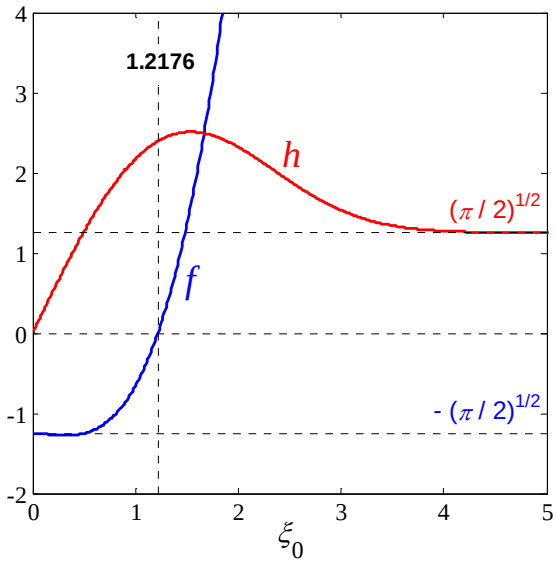

Fig. 8. The variation of functions *f* and *h* with ξ_0.

$$P_A^+ = C_2\left[\frac{1}{2} + \frac{\lambda_3}{6\pi}\{\xi_0^3 - \xi_0 - \sqrt{\frac{\pi}{2}}\,\exp(\xi_0^2/2)\,erfc(\xi_0/\sqrt{2})\}\right]. \tag{22}$$

The variation of this probability with ξ_0 and λ_3 is shown in Fig. 13, and its comparisons with the WACSIS data in Fig. 14. Note that $P_A^- \equiv \Pr\{\eta \le 0\,|\,A\}$ follows from $1 - P_A^+$ in both figures. By substituting (16) through (18) in (15), it is easily verified that $P_A^+ \to 1$ and $P_A^- \to 0$ as $\xi_0 \to \infty$. Further, Fig. 13 suggests that these limits are nearly realized for $\xi_0 \ge 6 \sim 8$, depending on λ_3.The WACSIS comparison in Fig. 14 confirms this observation and the predictions from (22), if allowance is made for the scarcity of the observed surface displacements when $\xi_0 > 4$. All this formalizes probabilistically the nature of large surface displacements, and that very large displacements can occur only above the mean sea level.

LARGE WAVES

Let m_j $(j = 0, 1, 2, \ldots)$ represent the ordinary spectral moments such that $m_0 = \sigma^2$, $\omega_m = m_1/m_0 \equiv$ spectral-mean frequency, and $\nu = [(m_0 m_2/m_1^2) - 1]^{1/2} \equiv$ spectral bandwidth. To the leading order of approximation, $\dot{\xi} \equiv \partial\xi/\partial t$ is independent of ξ and normally distributed with mean zero and standard deviation $\nu\omega_m$, viz. $p_{\dot{\xi}} \approx N(0; \nu\omega_m)$ for brevity. To the same order, $\dot{\phi} \equiv \partial\phi/\partial t$ is independent of $\dot{\xi}$, but not of ξ:

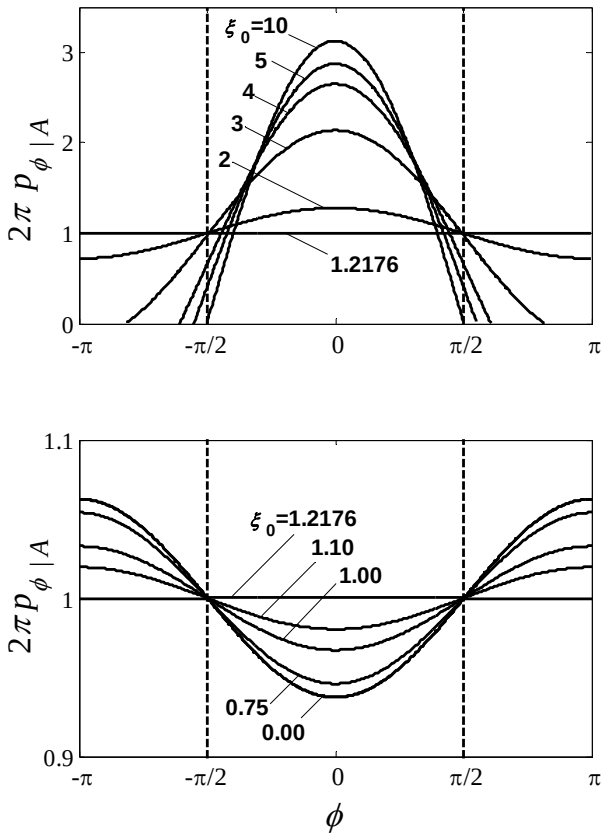

Fig. 9. The variation of the conditional p.d. $p_{\phi|A}$ of ϕ, given $A \equiv \{\xi > \xi_0\}$, with ξ_0 for $\lambda_3 = 0.3$.

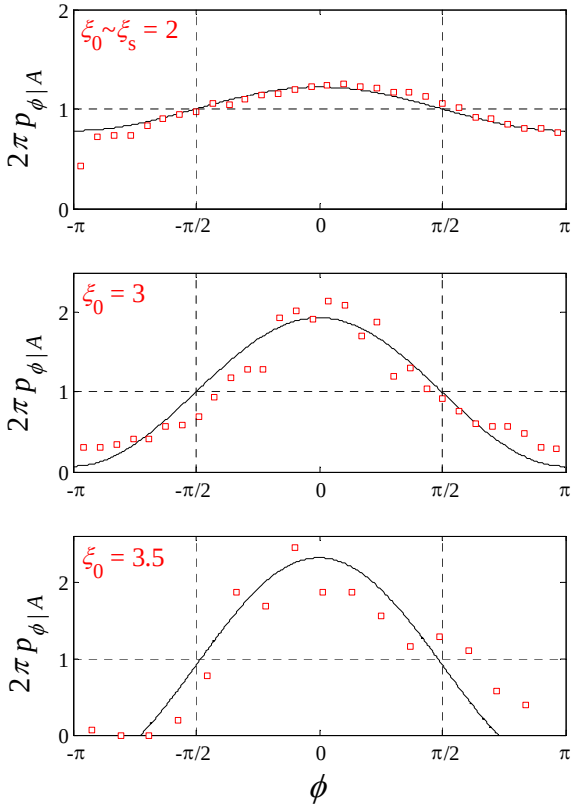

Fig. 10. Comparisons of the conditional p.d. $p_{\phi|A}$ of ϕ, given $A \equiv \{\xi > \xi_0\}$, observed in WACSIS with (15) for various ξ_0.

its conditional p.d. is $p_{\dot{\phi}|\xi} \approx N(\omega_m; \nu\omega_m/\xi)$, given ξ (Rice 1944, 1945; Longuet-Higgins 1957). In theory, these approximations are modified by nonlinear corrections of $O(\lambda_3)$, but the WACSIS data show that these are practically negligible. So, if ν is used as an ordering parameter, then ϕ and $\dot{\phi}$ are $O(1)$, and $\dot{\xi}$ is $O(\nu)$. At the positive extrema, $\eta > 0$, $\dot{\eta} = 0$, $\cos\phi = 1/\sqrt{1+(\dot{\xi}/\xi\dot{\phi})^2}$ and $\sin\phi = \pm(\dot{\xi}/\xi\dot{\phi})/\sqrt{1+(\dot{\xi}/\xi\dot{\phi})^2}$. Thus, $\cos\phi \to 1$ and $\sin\phi \to 0$ as $\xi \to \infty$, in which case $\eta \to \infty$ *and* $\hat{\eta} \to 0$ also. These theoretical limits signify that wave focusing is complete in that the phases of *all* spectral components approach zero simultaneously. Obviously, the probability for such occurrences is nil. In practice, for $\xi >> 1$, $\max \eta \to \xi + O(\nu/\xi)^2$ and $\hat{\eta} \to 0 + O(\nu/\xi)$. Under the same condition, ϕ increases monotonously since $\dot{\phi} > 0$. These conditions do in fact occur in WACSIS whenever $\xi > 1.5 - 2$,

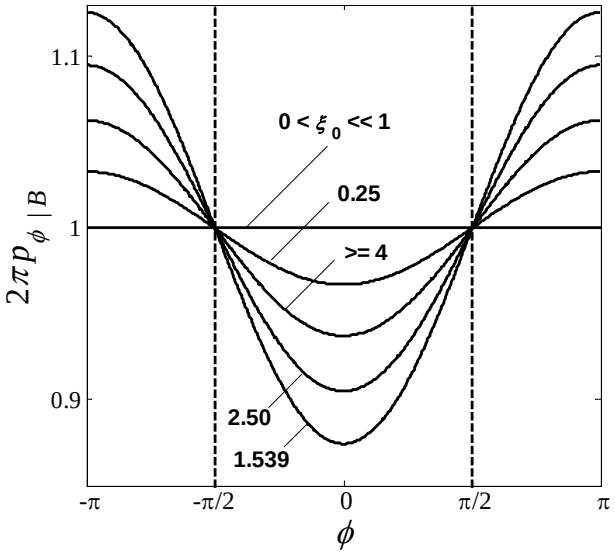

Fig. 11. The variation of the conditional p.d. $p_{\phi|B}$ of ϕ, given $B \equiv \{\xi \le \xi_0\}$, with ξ_0 for $\lambda_3 = 0.3$.

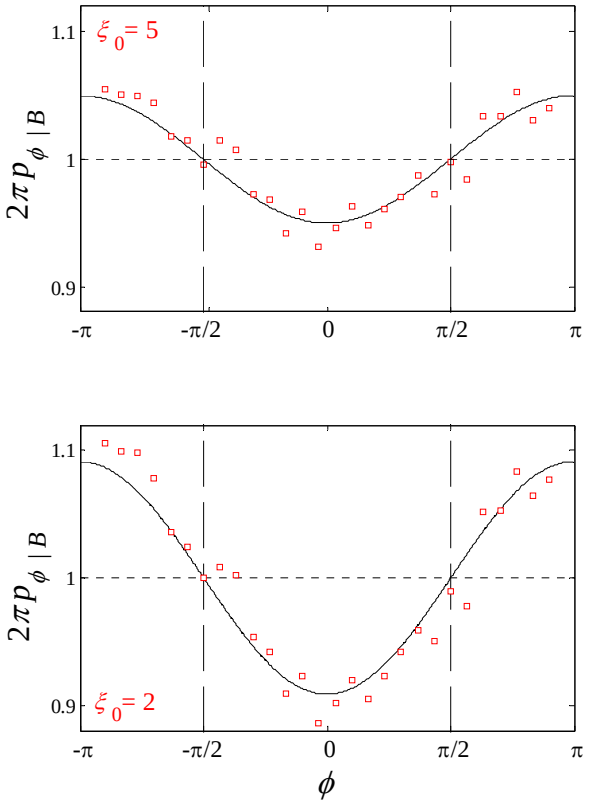

Fig. 12. Comparisons of the conditional p.d. $p_{\phi|B}$ of ϕ, given $B \equiv \{\xi \le \xi_0\}$, observed in WACSIS with (20).

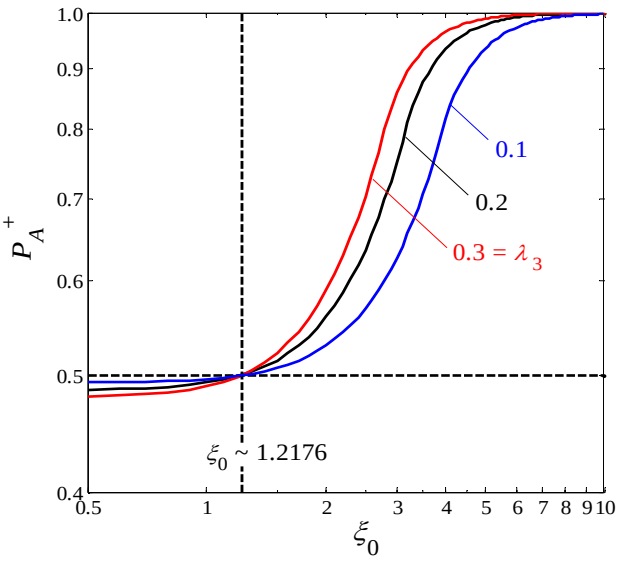

Fig. 13. The variation of the probability $P_A^+ = \Pr\{\eta > 0 \mid A\}$, given $A \equiv \{\xi > \xi_0\}$, with ξ_0 for $\lambda_3 = 0.1$, 0.2 and 0.3.

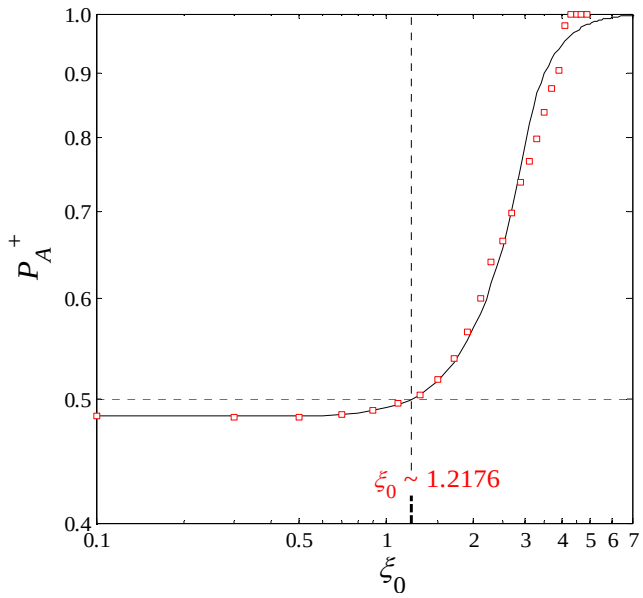

Fig.14. Comparison of $P_A^+ = \Pr\{\eta > 0 \mid \xi > \xi_0\}$ observed in WACSIS with the theoretical expression (22).

approximately. Physically, the corresponding surface profile and thus large waves appear more regular or narrow-banded: they do not display any secondary maxima or minima, but a single dominant crest proceeded by a relatively deeper trough. Secondary extrema can occur only during phase reversals when $\dot{\phi} < 0$. All this is illustrated in Fig. 15, where $\xi > 2$ around the largest wave in WACSIS, and in Fig. 16, where $\xi < 2$ approximately, for a 30-s segment of the surface time series near the beginning of the WACSIS measurements.

The theoretical models describing the expected shape of large waves, linear and nonlinear, are described in several studies. These include Lindgren (1972), Boccotti (1989, 2000), Phillips et al. (1993), and Tayfun & Fedele (2007a). In the linear case, the surface profile near a large wave crest is approximated by the conditional expectation

$$\langle\, \eta(t) \mid \xi_c >> 1 \,\rangle \cong \xi_c\, \rho(t)\,, \tag{23}$$

where $\xi_c = \eta(0) = \eta_{\max} \equiv$ wave crest, and $\rho \equiv$ normalized autocovariance of η. The corresponding wave height scaled with σ, say h, and the wave crest relate to one another as

$$\xi_c \cong h / (1-a)\,, \tag{24}$$

where $a \equiv \rho(t^*) < 0$, and t^* represents the time at which the first minimum of ρ occurs (Boccotti 1989, 2000). When

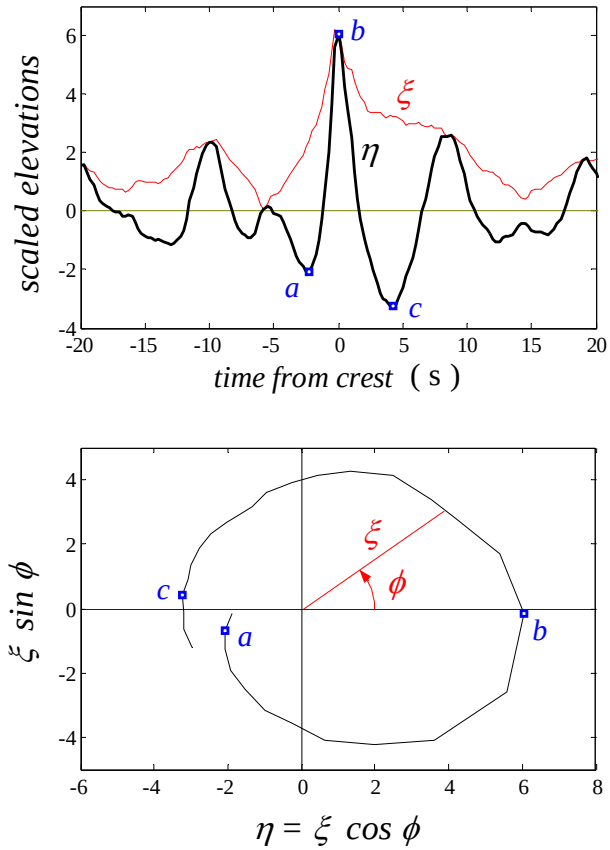

Fig. 15. The characteristics of the surface displacements, wave envelopes and phases around the largest wave where $\xi > 2$.

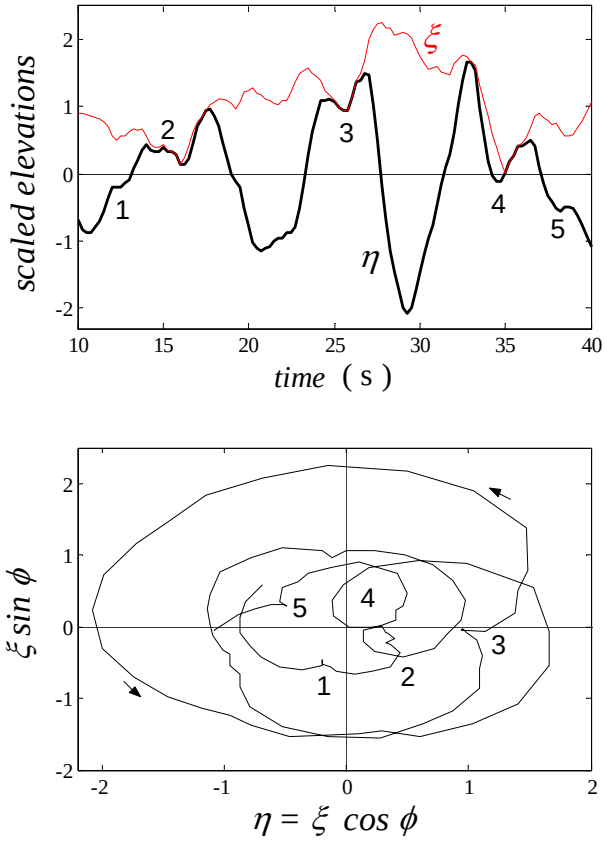

Fig. 16. Secondary maxima and minima associated with phase reversals when $\xi < 2$ approximately.

nonlinearities due to second-order bound waves become significant, (23) and (24) become (Tayfun & Fedele 2007a, b)

$$\langle \eta(t) \,|\, \eta(0) >> 1 \rangle \cong \xi_c \rho(t) + \frac{\lambda(t)}{6} \xi_c^2, \tag{25}$$

and

$$\eta_{\max} = \eta(0) \cong \xi_c \left(1 + \frac{\lambda_3}{6} \xi_c\right), \tag{26}$$

where $\lambda(t)$ is a dimensionless kernel: it has the functional form of a quadruple integral in terms of the directional spectral density of the sea surface and second-order interaction coefficients (c.f. Tayfun & Fedele 2007a,b). In general though, $\max \lambda(t) \le \lambda(0) = \lambda_3$, as a result of which (26) readily follows from (25).

The e.d.s of scaled zero-upcrossing wave heights *h*, crest ξ_c and trough ξ_t amplitudes observed in WACSIS are shown in Fig. 17. The e.d. estimate, say, E_j for the *j*-th largest value is based on the plotting position formula $\langle E_j \rangle = j/(N+1)$, where $N \equiv$ total wave count and j=1, 2, …, *N*. The standard deviation of E_j is (Tayfun & Fedele 2007b)

$$\sigma_{E_j} \cong \frac{1}{N+1} \sqrt{\frac{j\,(N-j+1)}{N+2}}\,. \tag{27}$$

For $N >> j$, $\sigma_{E_j} \cong \sqrt{j}/(N+1)$, which suggests that the variability of the e.d. estimates for the largest 5-10 samples can be rather large, as indicated by the $\pm\sigma_{E_j}$ error bands in Fig. 17. Most notably, σ_{E_1} is as large as E_1 itself, irrespective of how large *N* is.

The theoretical approximations describing e.d.s of scaled wave heights, crests, and trough amplitudes are reviewed in Tayfun & Fedele (2007b). For large waves, these include the following relatively simple expressions:

$$E_h = \sqrt{\frac{1+r_m}{2r_m}}\,\exp\left(-\frac{h^2}{4(1+r_m)}\right), \tag{28}$$

$$E_{\xi_c} = \exp\left[-\frac{1}{2}\left(\frac{\sqrt{1+2\mu_{F2}\xi_c}-1}{\mu_{F2}}\right)^2\right], \tag{29}$$

$$E_{\xi_t} = \exp\left[-\frac{\xi_t^2}{2}\left(1+\frac{1}{2}\mu_{F2}\,\xi_t\right)^2\right], \tag{30}$$

where r_m and μ_{F2} represent dimensionless wave-height and steepness parameters elaborated in Tayfun & Fedele (2007b) and Tayfun (2006), respectively. For WACSIS, $r_m = 0.699$ and $\mu_{F2} = 0.099$. The corresponding predictions from (28), (29) and (30) are compared with the WACSIS data in Fig. 17. Also included in these comparisons are $E_\xi = \exp(-\xi^2/2)$ for linear crest and trough amplitudes, and $E_{2\xi} = \exp(-h^2/8)$ for wave heights based on $h \cong 2\xi$, both of which are valid as $\nu \to 0$. Clearly, (30) describes the observed trough amplitudes quite accurately over all waves. Discrepancies do appear between the theoretical approximations (28) and (29) and the observed wave heights and crests of large waves characterized with relatively large variability. This is particularly so for the largest wave with a coefficient of variability of 100% since $\sigma_{E_1} \approx 1/(N+1)$ and $\langle E_1\rangle = 1/(N+1)$. As a result, $\Pr\{E \le \langle E\rangle - n\sigma_E\} = 0$ whereas $\Pr\{E > \langle E\rangle + n\sigma_E\} > 0$ for $n \ge 1$, suggesting that the largest wave observed is more likely to be biased toward larger frequencies of occurrence relative to theoretical predictions, as in WACSIS.

The theoretical mean and standard deviation of the largest value, say *Z*, in a population of *N* independent samples have the general forms (cf. Tayfun & Fedele 2007b)

$$\langle Z\rangle = \sqrt{\frac{\ln(c_0 N)}{c_1}} + \frac{\gamma}{2\sqrt{c_1 \ln(c_0 N)}}, \tag{31}$$

$$\sigma_Z \cong \frac{\pi}{2\sqrt{6c_1 \ln(c_0 N)}}, \tag{32}$$

where $\gamma = 0.577216... \equiv$ Euler's constant, $c_0 = 1/4(1+r_m)$ and $c_1 = \sqrt{(1+r_m)/2r_m}$ for the largest wave height in *N* waves, each described by a parent distribution of the form (28).

For the largest wave crest in *N* waves, (31) and (32) are modified to read

$$\langle Z_{\xi_c}\rangle \cong \langle Z\rangle + \frac{1}{2c_1}\mu_{F2}\,[\gamma + \ln(c_0 N)], \tag{33}$$

$$\sigma_{Z_{\xi_c}} \cong \sigma_Z\,[1+\mu_{F2}\sqrt{\ln(c_0 N)/c_1}] \tag{34}$$

where $c_0 = 1$ and $c_1 = 1/2$, assuming that each crest amplitude is described by (29). For WACSIS, $\langle Z\rangle \approx 7.89$ from (31) versus 9.27, the largest wave height observed; and, (33) gives $\langle Z_{\xi_c}\rangle \approx 5.16$ versus nearly 6.04 for the largest crest observed. Thus, the observed values are underestimated about 15% by the theoretical approximations, which are shown in Fig. 17 also, together with the corresponding errors bars $\pm\sigma_Z$ and $\pm\sigma_{Z_{\xi_c}}$.

Wave heights derived from zero-downcrossings can differ noticeably from the zero-upcrossing wave heights, in particular, over large waves. Wave crests remain the same in either definition, but the zero-upcrossing wave height is the sum of a crest and the preceding trough amplitude, which tends to be typically smaller than the trough amplitude following the same crest, as previously mentioned. Thus, zero-downcrossing wave heights can be expected to be somewhat smaller than the corresponding zero-upcrossing heights over large waves. This is evident in the comparisons of the WACSIS data in Fig. 18, where the largest zero-downcrossing wave height observed is 8.10, which compares more favorably to $\langle Z\rangle \approx 7.89$ from (31).

MICHE-STOKE LIMITS

In wind seas such as WACSIS, ρ has the form of a slowly decaying modulated narrow-band wave with no secondary maxima or minima. Evidently, this is consistent with the observed profile of surface displacements around a large wave crest, as seen here in WACSIS and in numerous other cases described in Phillips et al (1993) and Tayfun & Fedele (2007a). But, how large surface displacements and thus wave heights and crests can really become is a difficult question, particularly, based on the present theoretical model or higher-order approximations that ignore surface stresses, wave breaking and turbulent dissipation. The observation that wind-wave spectra tend to a ω^{-4} power law over high frequencies suggests that surface gradients are discontinuous in the mean-square sense. Thus, some waves reach a limiting steepness, display sharply cornered crests, and some break, forming whitecaps. An upper limit to wave steepness and thus wave heights is described by the Miche limit (Miche1944), given in the present notation by

$$h_{\max} = \frac{2\pi}{7\sigma}\frac{\tanh kd}{k}, \tag{35}$$

where $k \equiv$ wave number and $d \equiv$ mean water depth. As $d \to \infty$, (35) converges to the Stokes limit.

The applicability of the Miche-Stokes type limits to irregular waves has been the subject of numerous studies. These are reviewed in Tulin & Li (1992) and references therein. The Miche-Stokes limits or their various refinements do not appear as consistent indicators of wave breaking or its inception for irregular waves. However, they do indicate an upper bound to the heights of large waves, breaking or otherwise. The largest wave heights in WACSIS, shown in the upper part of Fig. 19 versus the corresponding scaled zero-upcrossing periods $\tau \equiv T/T_m$, where $T_m = 2\pi/\omega_m$, do not violate (35). Similarly, the lower part of the same figure shows the scatter of wave crests and the associated scaled periods in comparison with the approximate limits, say $\xi_{c\,\max 1}$ and $\xi_{c\,\max 2}$, which simply follow from (23) and (25), respectively, by replacing h with the Miche limit $h_{\max}$ of (35) as

$$\xi_{c,\ \max 1} = h_{\max}/(1-a)\,, \tag{36}$$

and

$$\xi_{c,\ \max 2} = \frac{h_{\max}}{1-a}\left(1+\frac{\lambda_3}{6}\frac{h_{\max}}{1-a}\right). \tag{37}$$

With $a = -0.661$ as an overall average value estimated from WACSIS, none of the preceding limits, not even the less conservative approximation (36) is violated by the largest wave crests or surface displacements. When $\xi < 2$ approximately, some waves do exceed the upper limits somewhat, but their profiles do not appear as regular or narrow-banded as in larger waves.

The mean $\langle \tau \,|\, h \rangle$ and standard deviation $\sigma_{\tau|h}$ of wave periods, conditional on $h >> 1$, are described reasonably well by the empirical approximations (Tayfun 1993)

$$\langle \tau \,|\, h \rangle \cong 1 + \frac{\nu^2}{(1+\nu^2)^{3/2}}\,, \tag{38}$$

$$\sigma_{\tau|h} \cong \frac{2\nu}{h\,(1+\nu^2)^2}\,. \tag{39}$$

As shown in Fig. 20, both expressions appear to approximate the WACSIS data well for large wave heights. On this basis, (38) can be used in the Miche-Stokes type upper limits to estimate the largest possible wave heights and surface displacements. This approach gives $h_{\max} \approx 11.07$ from (35) and $\xi_{c,\ \max 1} \approx 6.62$ from (36) as the largest possible theoretical expectations in comparison with, respectively, 9.27 and 6.04 actually observed in WACSIS. The theoretical $\xi_{c,\ \max 1}/h_{\max} \equiv 1/(1-a) \approx 0.60$ appears reasonable, but it underestimates the observed ratio $6.04/9.27 \approx 0.65$ of WACSIS largely because (36) tends to underestimate crest heights over large waves somewhat, as seen in Fig. 18. The estimate $\xi_{c,\ \max 2} \approx 8.41$ from (37) is larger than 6.04 observed, and it also suggests the more conservative ratio

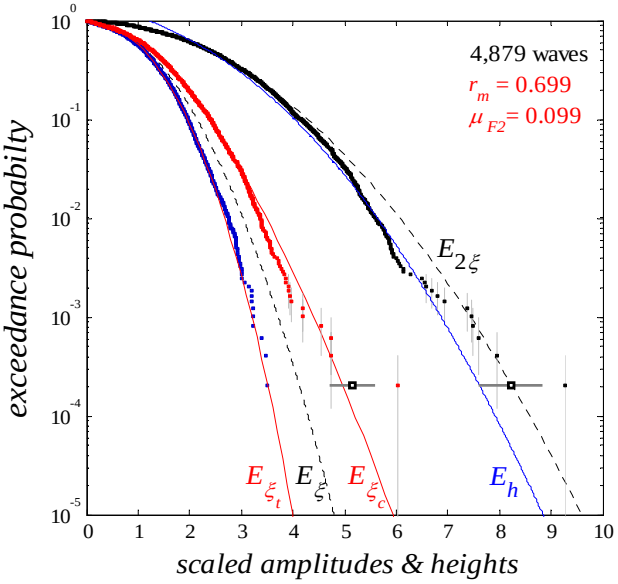

Fig. 17. Zero-upcrossing wave heights (h), crest (ξ_c) and trough (ξ_t) amplitudes observed in WACSIS in comparison with the theoretical approximations (28), (29) and (30).

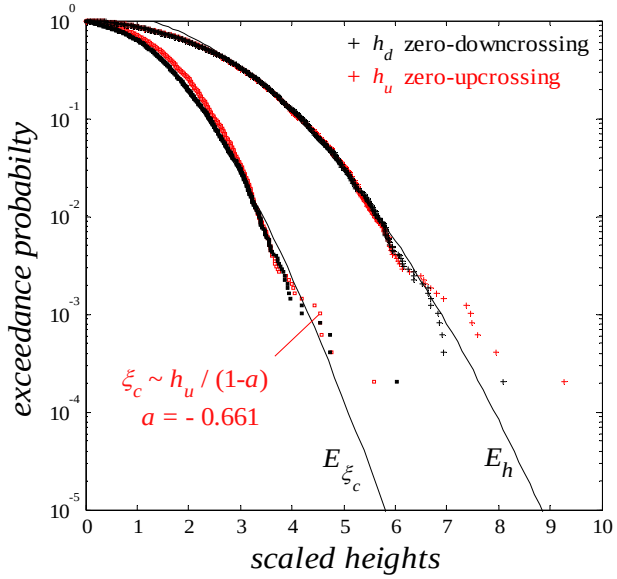

Fig. 18. Comparisons of zero up- and down-crossing wave heights h_u (+) and h_d (+), and crest heights ξ_c (•) observed in WACSIS, and the crest heights predicted from $h_u/(1-a)$ (•).

$$\frac{\xi_{c,\ \max 2}}{h_{\max}} = \frac{1}{1-a}\left(1+\frac{\lambda_3}{6}\frac{h_{\max}}{1-a}\right) \approx 0.76\,. \qquad (40)$$

THIRD-ORDER EFFECTS

In weakly nonlinear seas, third-order corrections to the surface displacements, wave envelopes and phases are all of $O(\lambda_3^2)$ and thus negligible. The favorable nature of the WACSIS comparisons tends to confirm this for the most part. If, however, quasi-resonant interactions between free waves become at least as significant as the second-order effects, surface statistics tend to deviate significantly from the second-order predictions. Such deviations are generated in lab flume experiments or numerically simulated under rather special conditions, generally requiring that waves be sufficiently long-crested and narrow-banded (cf. Socquet-Juglard et al. 2005, Mori et al. 2007). Mori & Janssen (2006) and Mori et al. (2007) formalize these conditions using the Benjamin-Feir-Index (*BFI*), which can be expressed in the present notation as

$$BFI \equiv \sqrt{2}\ \sigma\ k_m / \nu\,, \qquad (41)$$

where k_m satisfies $\omega_m^2 = g\,k_m \tanh k_m d$ with $g \equiv$ gravitational acceleration. In the deterministic theory, instabilities arise when $k_m d > 1.36$ *and* $BFI > 1$, but it is not clear if these thresholds are also valid for (41). Since awkward ambiguities arise in expressing k in terms of integral spectral properties of wind seas at shallower depths, it may be more reasonable to interpret the condition $k_m d > 1.36$ in terms of zero-crossing wave characteristics instead. As for *BFI*, the wave-flume data in Fig. 5 of Mori et al. (2007) coupled with their approximate equation (5) suggests that instabilities due to third-order interactions between free waves tend to become significant when $BFI > 0.5$ approximately.

Wind seas are neither long-crested nor narrow-banded, except possibly when they encounter spatially varying currents which can modify the sea surface significantly and cause waves to appear long-crested and narrow-banded (Tayfun et al. 1976). Further, modulations associated with third-order instabilities tend to follow a rather predictable and systematic pattern: they first appear at wave-height and crest levels near their significant values and then rapidly amplify over larger waves. This pattern is predicted well by the higher-order Gram-Charlier expansions describing the distributions of wave envelopes, wave heights and crests (Tayfun & Lo 1990, Mori et al. 2007, Tayfun & Fedele 2007b). For example, the marginal e.d. of wave heights $h \cong 2\xi$ in narrow-band waves is approximated by

$$E_h = e^{-h^2/8}\left[1+\frac{\Lambda}{1024}\,h^2(h^2-16)\right], \qquad (42)$$

where

$$\Lambda = \lambda_{40} + 2\lambda_{22} + \lambda_{04}\,, \qquad (43)$$

and $\lambda_{(4-n)n} = \langle \eta^{4-n}\hat{\eta}^{n}\rangle + (-1)^{n/2}(3-n)(n-1)\,;\ n = 0, 1, \ldots, 4$

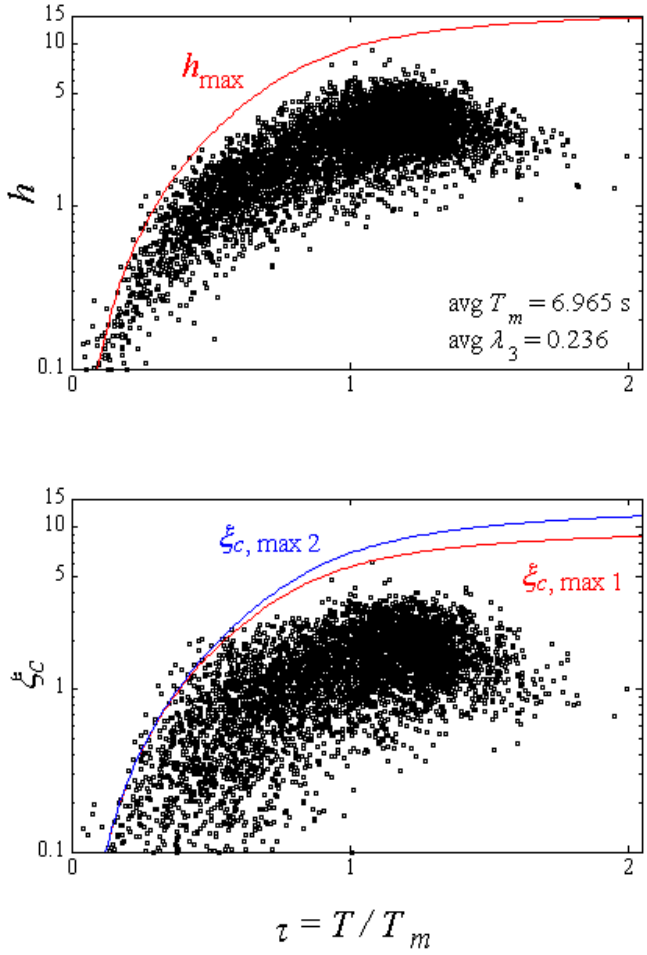

Fig. 19. The scatter diagrams of wave periods τ versus wave heights h and crests ξ_c observed in WACSIS in comparison with the Miche limit (35) and approximateions (36) and (37).

represent the fourth-order joint cumulants. For $\nu << 1$, the e.d. of wave heights in linear and second-order waves is described by the leading term $\exp(-h^2/8)$ in (42). The corresponding significant wave height is $h_s = 4$. For $\Lambda > 0$ and $h \geq h_s$, $E_h / \exp(-h^2/8) \geq 1$ and increases monotonously. Thus, (42) for wave heights and similar approximations in Tayfun & Fedele (2007b) for crest and trough amplitudes all suggest that over the range where significant values are exceeded, third-order instabilities systematically amplify wave heights, and crest and trough amplitudes noticeably and, if $\Lambda > 1$ approximately, well beyond the levels predicted by the linear and second-order approximations.

For wave phases, third-order corrections introduce several additional terms in (7). These are proportional to the fourth-order cumulants $\lambda_{(4-n)n}$ $(n = 0, 1, \ldots, 4)$ (Tayfun & Lo 1990).

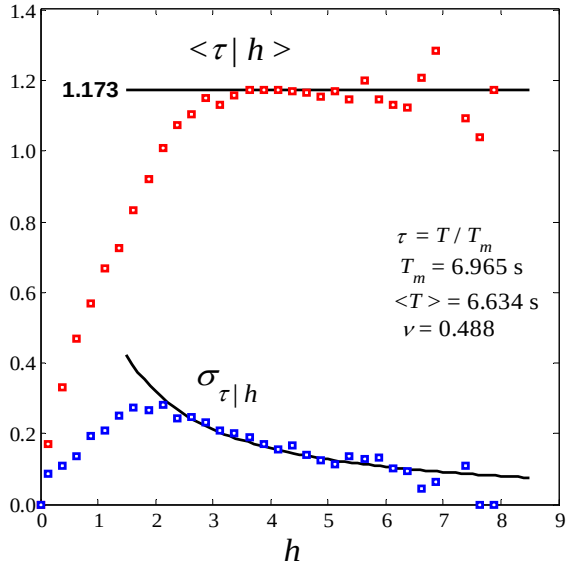

Fig. 20. Comparisons of the conditional mean and standard deviation of scaled wave periods observed in WACSIS with approximations (38) and (39).

As a result, (7) is modified as

$$
\begin{aligned}
2\pi\, p_\phi = 1 &- \frac{\lambda_3}{6}\sqrt{\frac{\pi}{2}}\cos\phi \\
&+ \frac{\lambda_{40}}{24}\,(8\cos^4\phi - 12\cos^2\phi + 3) \\
&+ \frac{\lambda_{22}}{4}\,(8\cos^2\phi\sin^2\phi - 1) \\
&+ \frac{\lambda_{04}}{24}\,(8\sin^4\phi - 12\sin^2\phi + 3),
\end{aligned}
\qquad (44)
$$

where it was assumed that $\lambda_{31} = \lambda_{13} \cong 0$, as in WACSIS . If, in addition, $\lambda_{22} \cong \lambda_{40}/3$ and $\lambda_{04} \cong \lambda_{40}$ also, as in Mori & Janssen (2006), then $\Lambda \to \Lambda_{app} \equiv 8\lambda_{40}/3$, and (44) identically reduces to (7).

The temporal variations of λ_{40}, λ_{22}, λ_{04}, Λ, Λ_{app} and *BFI* estimated as half-hourly running averages from WACSIS are shown in Fig. 21. The *BFI* estimates lie in a fairly narrow range from 0.186 to 0.320. As an overall average, $BFI \cong 0.25$. For the largest waves, $\langle \tau \mid h \rangle \approx 1.173$ from Fig. 20 leads to $kd \approx 1.27$. These do not provide any particularly strong evidence for the presence of third-order instabilities. The fourth-order cumulants appear to be rather unstable and spike occasionally above the overall averages. Such spikes always occur as they are expected to whenever the running averages include relatively large surface displacements, as indicated in the same figure by the six largest values η_j (j = 1, 2, .., 6) of WACSIS. Similar spikes and even larger ones are also observed in simulated series of perfectly linear Gaussian surface displacements under similar conditions (cf. Tayfun & Fedele 2007b). They simply reflect the highly variable nature of fourth-order cumulants and the difficulty of estimating them from relatively short time series. Thus, neither the BFI estimates nor the nature of fourth-order cumulants from WACSIS provide any clear evidence that the largest wave has anything to do with third-order instabilities. If they did, the largest wave would not just be an isolated outlier or a relatively rare occurrence captured by this particular set of measurements. It would instead appear as a realization in a larger population of waves that follow the systematic pattern alluded to earlier. The same conclusion is also valid for the wave-phase statistics observed in WACSIS: the average values of fourth-order cumulants are either slightly negative or negligible. Further, Fig. 21 shows that $\Lambda \cong \Lambda_{app}$, which in effect simplifies (44) to (7).

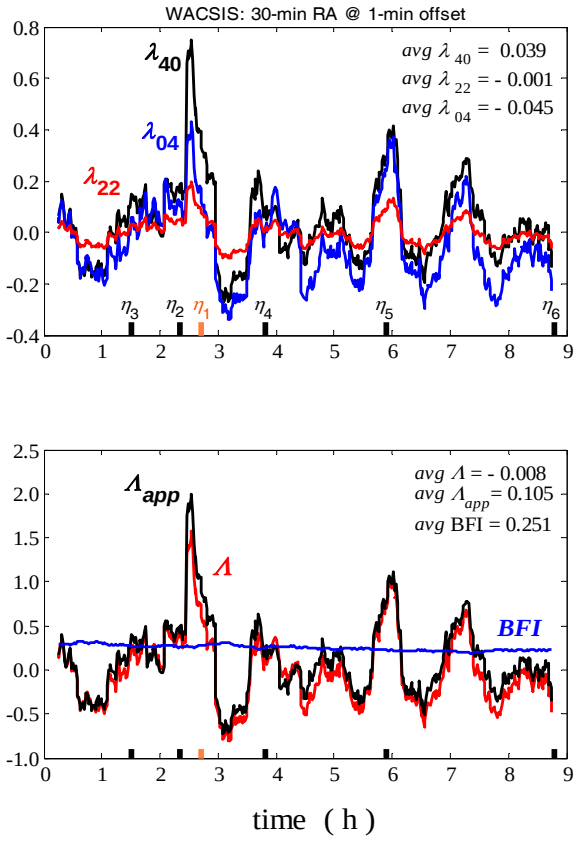

Fig. 21. Temporal variations of λ_{40}, λ_{22}, λ_{04}, Λ, Λ_{app} and *BFI* in WACSIS.

CONLUSIONS

The validity of theoretical approximations developed for describing the joint, marginal and conditional statistics of the envelope and phase of wind waves characterized by second-

order nonlinearities is confirmed by the WACSIS comparisons. The theoretical results also suggest that wave-phase statistics and the nature of surface displacements tend to differ appreciably but predictably, depending on whether if envelope elevations exceed the significant envelope height or not. For elevations sufficiently larger than this particular threshold, wave-phase distributions approach a simple limit form which shows that large surface displacements can occur only above the mean sea level. This is likewise confirmed by the WACSIS data.

Larger waves appear more regular or narrow-banded than relatively low waves, and their heights and crests do not exceed the Miche-Stokes type upper limits. This appears to be so even for unusually large waves with scaled features and proportions similar to the largest wave captured in the WACSIS measurements. The constructive interference of spectral components with different amplitudes and phases is the most likely mechanism that generates large surface displacements and thus such large waves under oceanic conditions. Third-order nonlinearities, if any, including quasi-resonant interactions between free waves, do not appear to affect the observed statistics in any discernable way.

The largest wave in WACSIS is likely to be a relatively rare occurrence. It would not have appeared so unusual, had the measurements been maintained sufficiently longer or, if many more wave probes had been deployed to gather an ensemble of simultaneous measurements. Because of the highly unstable nature of statistics associated with the largest observations, a sample population of about 5,000 waves gathered at a fixed point in time may not always be adequate for reliably estimating the occurrence frequencies of such exceptionally large waves.

ACKNOWLEDGMENTS

The author is indebted to G..Z. Forristall, Ocean Engineering, Inc., Camden, ME, USA, and M. Prevosto, Ifremer, for the WACSIS data.

REFERENCES

Al-Humoud, J., M.A. Tayfun, and H. Askar, 2002: Distribution of nonlinear wave crests. *Ocean Eng*., **29,** 1929- 1943.

Boccotti, P., 1989: On mechanics of irregular gravity waves. Atti Academia Nazionale dei Lincei, Memorie VIII, **19**, 111-170.

Boccotti, P., 2000: *Wave Mechanics for Ocean Engineering*. Elsevier Science, New York, 405 pp.

Cherneva, Z., P. Petrova, N. Andreeva, and C. Guedes Soares, 2005: Probability distributions of peaks, troughs and heights of wind waves measured in the Black Sea coastal zone, *Coastal Eng*., **52**, 599-615.

Forristall, G. Z., H. E. Krogstad, P. H. Taylor, S. S. Barstow, M. Prevosto, and P. Tromans, 2002: Wave crest sensor intercomparison study: an overview of WACSIS. *Proc., 21st Int. Conference on Offshore Mechanics and Arctic Engineering*, American Society of Mechanical Engineers, paper no. OMAE2002-28438, pp. 1-11.

Lindgren, G. 1972: Local maxima of Gaussian fields. *Arkiv förMatematik* **10**, 195-218.

Longuet-Higgins, M.S., 1957: The statistical analysis of a random moving surface. *Phil. Trans. R. Soc. London*, Ser. A, **966**, 321-387.

Miche, R., 1944: Mouvements ondulatoires de la mer en profoundeur constante ou decroissante. Annales des Ponts et Chaussees, **121**, 285-318.

Mori, N., and P. A. E. M. Janssen, 2006: On kurtosis and occurrence probability of freak waves. *J. Phys. Oceanogr*., **36**, 1471-1483.

Mori, M., M. Onorato, P. A. E. M. Janssen, A. R. Osborne, and M. Serio, 2007: On the extreme statistics of long-crested deep water waves: Theory and experiments. *J. Geophys. Res***., 112**, C09011 10.1029/2006JC004024.

Phillips, O. M., D. Gu, and M. Donelan, 1993: Expected structure of extreme waves in a Gaussian sea. Part I: theory and SWADE buoy measurements. *J. Phys. Oceanogr*. **23**, 992-1000.

Rice, S. O., 1944: The mathematical analysis of random noise. *Bell System Tech. J*., **23**, 282-332.

Rice, S. O., 1945: The mathematical analysis of random noise. *Bell System Tech. J*., **24**, 46-156.

Socquet-Juglard, H., K. Dysthe, K. Trulsen, H. E. Krogstad, and J. D. Liu, 2005: Probability distributions of surface gravity waves during spectral changes. *J. Fluid Mech*., **542**, 195-216.

Tayfun, M.A., 1980: Narrow-band nonlinear sea waves. *J. Geophys. Res*., **85**, 1548-1552.

Tayfun, M. A., 1993: Joint distribution of large wave heights and associated periods. *J. of Waterway., Ports, Coastal Ocean Eng.*, **119**, 261-273.

Tayfun, M. A., 1994: Distributions of wave envelope and phase in weakly nonlinear random waves. *J. Eng. Mechanics*., **120**, 1009-1025.

Tayfun, M. A., 2006: Statistics of nonlinear wave crests and groups. *Ocean Eng.*, **33**, 1589–1622.

Tayfun, M.A., R. A. Dalrymple, and C.Y. Yang, 1976: Random wave-current interactions in water of variable depth. *Ocean Eng*., **3**, 403-420.

Tayfun, M. A., and F. Fedele, 2007a: Expected shape of large waves in storm seas. *Proc. 26th Int .Conference on Offshore Mech. and Arctic Eng.*, San Diego, CA, USA, American Society of Mechanical Engineers, paper no. OMAE2007-29073.

Tayfun, M. A., and F. Fedele, 2007b: Wave-height distributions and nonlinear effects. *Ocean Eng*., **34**, 1631-1649.

Tayfun, M.A., and J-M. Lo, 1989: Envelope, phase and narrow-band models of sea waves. *J. of Waterway., Ports, Coastal Ocean Eng.*, **115**, 594-613.

Tayfun, M. A., and J-M. Lo, 1990: Non-linear effects on wave envelope and phase. *J. of Waterway., Ports, Coastal Ocean Eng.*, **116**, 79-100.

Tulin, M.P., and Li, J.J., 1992: On the breaking of energetic waves. *Int. J. Offshore Polar Eng*., **2**, 46-53.

